

Article

Enhancement of the Vegetation Carbon Uptake by the Synergistic Approach to Air Pollution Control and Carbon Neutrality in China

Xiao Qin ^{1,2} , Guangming Shi ^{2,3,*}  and Fumo Yang ^{2,3}¹ Department of Environmental Science and Engineering, Sichuan University, Chengdu 610065, China² National Engineering Research Center on Flue Gas Desulfurization, Chengdu 610065, China³ College of Carbon Neutrality Future Technology, Sichuan University, Chengdu 610065, China

* Correspondence: shigm@scu.edu.cn

Abstract: Carbon sinks provided by land ecosystems play a crucial role in achieving carbon neutrality. However, the future potential of carbon sequestration remains highly uncertain. The impact of pollutant emission reduction (PER) introduced by the proposed synergistic approach to air pollution control and carbon neutrality on carbon sinks in China has not yet been fully evaluated. In this study, we analyzed the effects of regional carbon-neutral PER policies, global climate change, and their coupled effects on China's terrestrial gross primary productivity (GPP) by conducting numerical experiments using the weather research and forecasting model coupled with chemistry (WRF-Chem) and the moderate resolution imaging spectroradiometer photosynthesis algorithm (MODIS-PSN). We found that carbon-neutral PER policies could promote GPP growth in most regions of China in 2060, particularly during April and October, resulting in a total increase of at least 21.84 TgC compared to that in 2016, which offset the adverse effects of global climate change up to fourfold. The aerosol radiative effects drive GPP growth under carbon-neutral PER policies, primarily through an increase in daily minimum temperature during winter and an increase in shortwave radiation during other seasons. Our research highlights that reducing pollutant emissions enhances future potential for carbon sequestration, revealing positive feedback towards achieving the target of carbon neutrality.

Keywords: carbon-neutral pollutant emission reduction policies; gross primary productivity; aerosol radiative effects



Citation: Qin, X.; Shi, G.; Yang, F. Enhancement of the Vegetation Carbon Uptake by the Synergistic Approach to Air Pollution Control and Carbon Neutrality in China. *Atmosphere* **2024**, *15*, 578. <https://doi.org/10.3390/atmos15050578>

Academic Editor: Alexandra Monteiro

Received: 1 April 2024

Revised: 30 April 2024

Accepted: 4 May 2024

Published: 9 May 2024



Copyright: © 2024 by the authors. Licensee MDPI, Basel, Switzerland. This article is an open access article distributed under the terms and conditions of the Creative Commons Attribution (CC BY) license (<https://creativecommons.org/licenses/by/4.0/>).

1. Introduction

Climate change is an urgent global concern and one of the paramount challenges confronting the world today. The international community is actively engaged in efforts to tackle climate change [1]. This necessitates achieving carbon neutrality, which refers to attaining a balance between the net carbon dioxide (CO₂) emissions and removal or offsetting measures. Fundamentally, two primary approaches can be adopted to accomplish this objective: reducing carbon emissions and enhancing carbon sinks [2,3]. While technological advancements and policy interventions contribute significantly to emission reduction, harnessing the natural capacity of ecosystems to absorb and sequester carbon is equally indispensable [4].

The gross primary productivity (GPP) of terrestrial ecosystems is the largest component of the Earth's carbon cycle [5,6], as it determines the initial material and energy that land ecosystems obtain from external sources [7]. GPP serves as the primary pathway for terrestrial carbon exchange between land and atmosphere, playing a crucial role in regulating the Earth's carbon balance [8]. Capturing atmospheric CO₂ through vegetation photosynthesis is a vital strategy for achieving carbon neutrality [9]. Therefore, accurate estimation of GPP is essential for assessing the potential of terrestrial ecosystems to sequester carbon. Rising atmospheric CO₂ concentrations impact GPP in both direct and indirect

ways simultaneously. The direct way is mainly referred to as the CO₂ fertilization effect, suggesting that the increase in atmospheric CO₂ concentration stimulates the photosynthesis process [10,11]. However, the enhancement trend of carbon sink is slowing down and is projected to be averted in the future [12,13]. The indirect way represents the impact through modulating the environmental conditions, such as meteorological parameters and soil mineralization. For instance, variations in meteorological factors could result in a decrease in carbon sequestration potential. Future warming-induced extreme droughts may lead to losses in net primary productivity (NPP) [14]. Conversely, increased precipitation in wet regions could reduce temperatures and radiation, thereby suppressing vegetation growth. Additionally, an expanding atmospheric water vapor pressure deficit (VPD) might diminish vegetation productivity [15]. The combined impact of these factors makes the estimation of future carbon sink potential challenging.

The Chinese government has proposed achieving national carbon neutrality by 2060. Effective measures to reduce carbon emissions have been implemented and are planned for future implementation. Research indicates that air pollutants and greenhouse gas emissions share common roots, sources, and processes. Therefore, there is widespread attention from governments and scholars towards a synergetic approach to air pollution control and carbon neutrality [16,17]. Integrated scenarios for reducing anthropogenic air pollutant emissions have been proposed, such as the dynamic projection model for emissions in China (DPEC) dataset [18]. These carbon-neutral pollutant emission reduction (PER) measures impact the concentration of air pollutants [19], which further affect meteorological elements and influence vegetation growth through their radiative effects. However, the specific impact of this effect on vegetation carbon uptake remains unexplored.

In case of the ambiguous GPP variation trends caused by global climate change and CO₂ concentration rising [12–14,20], the feedback of PER measures on GPP becomes imperative for achieving the carbon neutrality goal, especially in rapidly developing and severely polluted regions such as China. This study aims to evaluate the impact of PER on GPP in China under the context of carbon neutrality. We coupled the weather research and forecasting model with chemistry (WRF-Chem) and the moderate resolution imaging spectroradiometer photosynthesis algorithm (MODIS-PSN) to simulate future GPP variation results from global climate change, PER measures, and their coupled effects. The results can reveal to what extent the proposed synergistic approach to air pollution control and carbon neutrality affects the vegetation carbon uptake through PER measures. The implications are valuable for policymaking while achieving carbon neutrality targets in China.

2. Materials and Methods

2.1. Meteorological and Chemistry Simulation

The meteorological parameters over China were simulated by the WRF-Chem model version 4.0 [21], which was jointly developed by the National Oceanic and Atmospheric Administration (NOAA) and the Earth System Research Laboratory (ESRL). The simulation domain covers mainland China, which is centered at (35° N, 103° E) and expands 165 and 150 grids with a grid spacing of 36 km along the zonal and meridional direction. The meteorological parameters were simulated by the model at 35 levels below 50 hPa. The simulation incorporated various physical parameterization schemes (Table 1), including the Yonsei University (YSU) planetary boundary layer scheme [22], the Noah land surface model [23], the Grell-3D cumulus convection scheme [24], the Morrison double-moment microphysics scheme [25], and the RRTMG shortwave and longwave radiation schemes [26]. To drive the WRF-Chem model, dynamic initial and boundary conditions were obtained from HighResMIP's (high-resolution model intercomparison project) climate projection (MPI-ESM1-2-HR) data of the CMIP6 (phase 6 of the coupled model intercomparison project), which had a grid resolution of 0.93° × 0.93° and were interpolated at 6 h intervals [27].

Table 1. Settings and parameterization schemes of WRF-Chem simulation.

Model Settings	Values
Horizontal resolution	36 km
Vertical resolution	35 eta levels up to 50 hpa
Domain size	165 × 150 grids
Meteorological boundary	MPI-ESM1-2-HR (0.94° × 0.94°, 6 h)
Chemical boundary	MOZART (0.9° × 1.25°, 6 h)
Physical Option	Parameterization Scheme
Microphysics	Morrison two-moment
Shortwave radiation	RRTMG
Longwave radiation	RRTMG
Surface layer	MM5 Monin-Obukhov
Land-surface	Noah
Boundary layer	YSU
Cumulus	Grell 3D
Chemical Option	Parameterization Scheme
Gas phase chemistry	CBMZ
Photolysis	Fast-J
Biogenic emissions	MEGAN
	MEICv1.3 (0.25° × 0.25°),
Anthropogenic emissions	MICS-ASIA III (0.25° × 0.25°),
	DPEC (0.25° × 0.25°)

Table 1 demonstrates the model input data and parameterization settings in this study. The CBMZ [28] and MOSAIC [29] mechanisms were employed for simulating gaseous and particulate chemistry. The initial and boundary conditions of atmospheric chemical compositions were derived from climatological chemical data obtained from the model for O₃ and related chemical tracers (MOZART) [30,31]. The anthropogenic emissions were derived from the multi-resolution emission inventory for China (MEIC) dataset version 1.3 [32,33] over mainland China and the model inter-comparison study for Asia (MICS-ASIA III) dataset [34] outside of China. The anthropogenic emissions in 2060 over China were derived from the carbon-neutral scenarios of the DPEC dataset [18]. Biogenic emissions were obtained from version 3 of the model of emission of gases and aerosols from nature (MEGAN) [35].

The simulated meteorological parameters (2 m temperature and 2 m relative humidity) and air pollutant concentrations (PM_{2.5} and O₃) in January, April, July, and October of 2016 were compared with the observations from 439 meteorological stations and 1425 state-controlled ambient air quality monitoring stations across China, respectively (see Tables S1 and S2). The meteorological simulation exhibited good model performance as evidenced by small average deviations between simulation results and observation data, such as mean fractional bias (MFB) ranging from −30% to 30%, mean fractional error (MFE) below 50%, as well as negligible normalized mean bias (NMB) and normalized mean error (NME). Regarding the air pollutant concentrations, both O₃ and PM_{2.5} concentrations exhibited MFBs within the range of −60% to 60%, while MFEs remained below 75%. Notably, O₃ simulation demonstrated superior performance in July with MFBs ranging from −30% to 30% along with MFEs below 50%. All NMB values were positive for both O₃ and PM_{2.5} concentrations over China, indicating a slight overestimation by the model. Consequently, the model successfully replicated variations in meteorological parameters as well as air quality [36].

2.2. Terrestrial GPP Calculation

Currently, the primary methods for calculating total primary productivity encompass statistical models, parametric models, and process models. Among these, process models based on light energy utilization are extensively employed. The global GPP product

derived from the moderate resolution imaging spectroradiometer (MODIS) [37] is arguably the most widely used worldwide GPP product [38], which is based on a light energy utilization model—the MODIS photosynthesis (PSN) algorithm developed by Running et al. [37]. Model parameter values are provided in the biome specified parameter look-up Table (BPLUT), which is designed to establish a physiological framework for regulating simulated carbon sequestration [39]. In this study, the meteorological parameters simulated by the WRF-Chem model served as inputs for the MODIS-PSN model to estimate GPP.

The daily terrestrial GPP in each simulation grid was calculated using the MODIS-PSN algorithm, which integrates absorbed photosynthetically active radiation (PAR) and the light energy utilization rate [37,40]. The absorbed PAR was estimated by multiplying the incident PAR from the model output with the absorbing fraction determined by the underlying plant canopy. The light energy utilization rate was obtained by querying the biological property lookup table based on vegetation cover type and adjusted for daily minimum temperature (Tmin) and the average difference between water vapor pressure at saturation and actual vapor pressure (VPD). The widely used IGBP classification system for land cover categorization was employed to estimate GPP in this study [41]. Comparisons with MYD17A2H product [42] revealed that this method successfully reproduced spatial patterns of GPP, exhibiting high correlation coefficients ($R = 0.59\text{--}0.78$, $p < 0.001$) and relatively low bias (nationwide RMSE < 78.56 gC/m²) (see Table S6).

2.3. Scenario Setting

Four sets of numerical experiments were carried out to examine the impact of the synergistic approach to air pollution control and carbon neutrality and global climate change on terrestrial GPP in China. As summarized in Table 2, the baseline (BL) for GPP in 2016 was simulated using meteorological fields and anthropogenic emissions from that year. The first control experiment (CN) assessed the impact of the synergistic approach to air pollution control and carbon neutrality by simulating meteorological fields from 2016 and projected anthropogenic emissions from 2060. The second control experiment (CC) evaluated the impact of global climate change by simulating projected meteorological fields from 2060 and anthropogenic emissions from 2016. The coupled effects of these two factors (CE) were simulated by considering projected meteorological fields and anthropogenic emissions from 2060. Four different shared socioeconomic pathways (SSPs) and representative concentration pathways (RCPs) [43] were considered for projecting future meteorological conditions, including SSP126 (SSP1 + RCP2.6, a green development pathway), SSP245 (SSP2 + RCP4.5, an intermediate development pathway), SSP370 (SSP3 + RCP7.0, a pathway between SSP245 and SSP585), and SSP585 (SSP5 + RCP8.5, a high development pathway).

Table 2. Scenario settings in the simulation of GPP.

Scenario Configuration	Meteorological Fields	Anthropogenic Emissions
BL	2016	2016
CN	2016	2060
CC	2060	2016
CE	2060	2060

2.4. Sensitivity Analysis

The Sobol sensitivity analysis method was employed to assess the relative importance of meteorological parameters, including Tmin, VPD, and near-surface shortwave radiation (Srad), in influencing variations of GPP. This approach represents a global sensitivity analysis technique based on variance decomposition that aims to quantify the contribution of each parameter's unconditional variance to the model output. Moreover, it has the capability to consider both individual parameter effects and their coupling influences [44]. In this study, 2000 samples were included in the Sobol sensitivity analysis for each grid.

These samples were randomly extracted from the GPP values falling in the range of monthly mean \pm standard deviation.

3. Results

3.1. The Projected Terrestrial GPP Variations

In terms of the total GPP during four representative months (January, April, July, and October), global climate change leads to declines in GPP of -39.69 TgC, -44.69 TgC, and -17.16 TgC under SSP126, SSP370, and SSP585 scenarios, respectively. However, a slight increase in GPP of 2.56 TgC is observed under the SSP585 scenario. The effect of global climate change exhibits distinct variations among different seasons and SSP scenarios as depicted in Figure 1 and Table S3. In January, GPP showed decreasing trends under most SSP scenarios, except for the SSP585 scenario under which a slight increase of 2.00% is observed. In April, increasing trends in GPP are observed under SSP245 and SSP585 scenarios, with increases of up to 6.35% . Conversely, decreasing trends occur under SSP126 and SSP370 scenarios by -0.60% and -2.96% , respectively. Decreasing trends in GPP are evident across all scenarios in July. Although the maximum relative reduction rate is only -4.62% under the SSP585 scenario, it represented the largest absolute reduction amount among the four months due to July having the highest baseline GPP value. In comparison, October showed increasing trends in GPP under most SSP scenarios by up to 8.00% , except for a decrease of 9.54% observed under the SSP245 scenario. Additionally, reductions caused by global climate change exceed -50.00 TgC as maximum amounts, which are relatively larger than increases that range around 40.00 TgC.

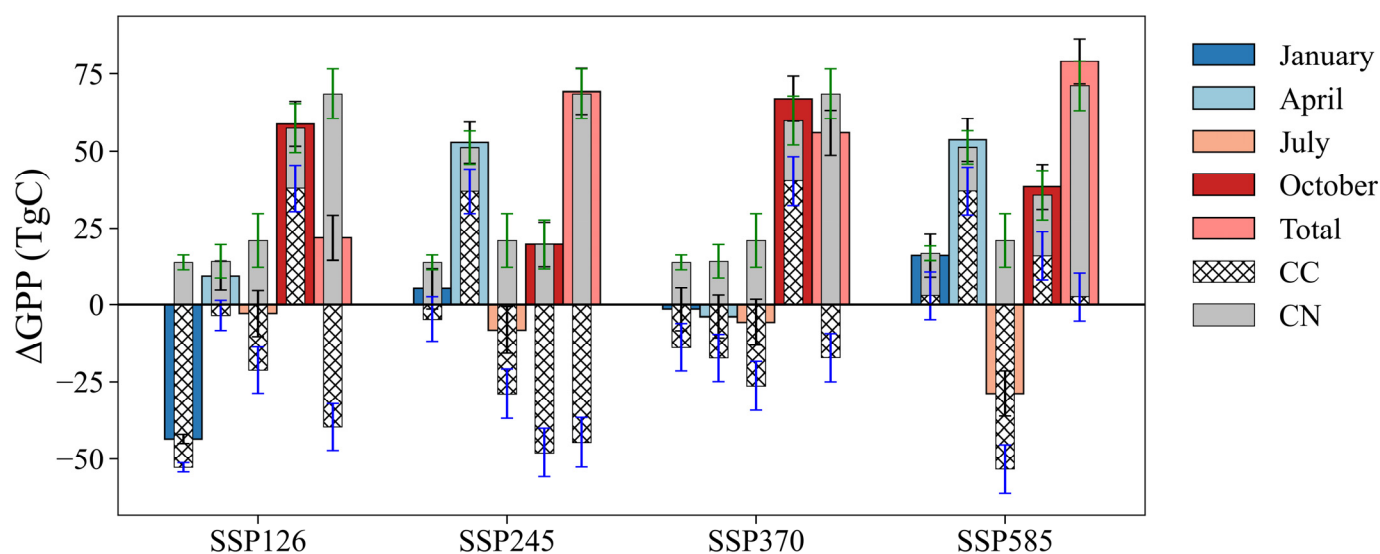


Figure 1. Changes in GPP under different scenarios. CN, CC, and CE represent the impact of PER only, global climate impacts only, and coupled effects of these two factors, respectively. Total represents the cumulative impact across four months. The blue, green, and black error bars represent the standard deviations of changes in GPP caused by CC, CN, and CE, respectively.

On the contrary, the PER results in a substantial increase in GPP of 68.63 TgC by 2060, accounting for 2.88% of the baseline and effectively offsetting the decline in GPP caused by climate change up to fourfold depending on SSP scenarios. The impact of PER on GPP exhibits slight seasonal variation, with larger increases observed in July (20.96 TgC) and October (19.65 TgC) compared to April (14.21 TgC) and January (13.81 TgC). Considering the larger baseline GPP in July and April as shown in Table S3, the relative variations of GPP present more obvious seasonal differences. PER leads to a significant growth in GPP by 9.40% in January in terms of relative variations, followed by 3.90% in October, while relatively smaller increments are observed in April (2.44%) and July (1.81%). The magnitude of GPP increases induced by PER is considerable when compared to the impacts

of global climate change alone. For example, during the four representative months, the GPP enhancements resulting from PER can offset the reductions caused by global climate change at rates of 1.73, 1.54, and 4.00 times under SSP126, SSP245, and SSP370 scenarios, respectively.

Resulting from the offset caused by PER, the GPP increases under most SSP scenarios considering the coupled effects of PER and global climate change. The maximum reduction in GPP is 43.53 TgC, occurring under the SSP126 scenario in January, accounting for 29.62% of the baseline GPP. Conversely, the maximum increase in GPP is significantly larger at 66.99 TgC and occurs under the SSP370 scenario in October, accounting for 13.31% of the baseline GPP. Notably, negative variations in GPP persist across all SSP scenarios due to positive contributions from PER in July.

In summary, global climate change will lead to a reduction in GPP under most SSP scenarios by 2060 compared to that in 2016; however, PER can significantly enhance GPP in 2060 and offset the decline caused by global climate change up to fourfold. This positive feedback of PER on GPP highlights the effectiveness of the synergistic approach to air pollution control and carbon neutrality towards achieving China's carbon neutral target.

3.2. Spatial Distribution Characteristics of the Projected Terrestrial GPP Variations

The spatial distribution of GPP across China in 2060 is significantly influenced by global climate change, as illustrated in Figure 2. In January, the regions experiencing a decrease in GPP are predominantly located in eastern China under the SSP126 scenario and gradually diminish with worsening climate conditions. The proportion of regions with declining GPP drops from 86% under the SSP126 scenario to 53% under the SSP585 scenario. Conversely, areas exhibiting an increase in GPP are primarily found in Yunnan Province and also appear along the southeastern coastal area under the SSP245 scenario. In April, contrasting spatial patterns emerged with decreasing GPP observed in Yunnan Province and increasing GPP observed elsewhere. In July, regions experiencing a decline in GPP are concentrated over the North China Plain (NCP), while significant increases occur over the Tibetan Plateau and southern China. The trend of GPP variation shifts from growth to decline for northeastern China between the SSP126 and SSP585 scenarios. In October, most regions of China witnessed an increase in GPP, accounting for approximately 70% of the study area; however, this does not hold true for southern China under both SSP245 and SSP585 scenarios. The reduction of GPP in southern China during October is consistent with the results projected by a machine learning method [45] and might be caused by the rising VPD in this region as shown in Figure S1 and discussed in Section 3.3 because extremely high VPD inhibits photosynthesis through closing plants' stomata [46].

Figure 3 depicts the spatial distribution of GPP changes resulting from PER in China. Notably, PER enhances GPP across most regions of China, with increasing areas accounting for at least 77% of the study area, particularly in January and October with the proportion exceeds 90%. The Sichuan Basin (SCB) in southwestern China exhibits a relatively high increase in GPP throughout all seasons under the influence of PER. Additionally, higher GPP-increasing regions cover southern China in January and October, the NCP and northeastern China in July, regions between the Yangtze River and the Yellow River in April, and the Yunnan–Guizhou Plateau (YGP) in October. The main decreasing regions appear over Yunnan Province in April and southern China as well as eastern Inner Mongolia during July.

In terms of the coupling effect of PER and global climate change (see Table S4 and Figure S1), Yunnan Province emerges as the primary region for GPP increase in January, accounting for 72% of the total GPP increment. However, it becomes the primary region for GPP reduction in April, with a decrease of 58.35 TgC. GPP growth is concentrated in the Hunan, Jiangxi, Heilongjiang, Henan provinces, and Inner Mongolia during this month. In July, the Tibet and Qinghai provinces contribute to over half of the total increase. Most provinces exhibit GPP growth under all SSP scenarios in October, with the highest increases observed in the SCB, Heilongjiang Province, and Inner Mongolia.

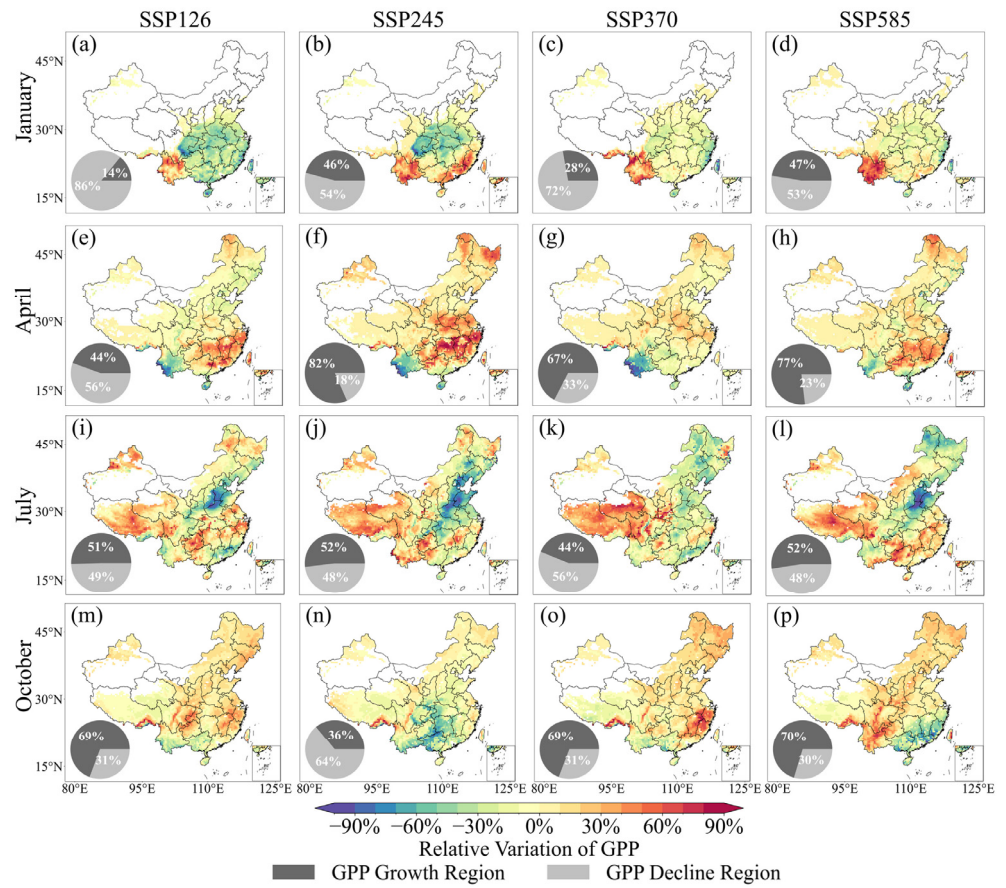


Figure 2. (a–p) Impact of global climate change on GPP. Pie charts indicate the proportions of the region with increasing and decreasing GPP.

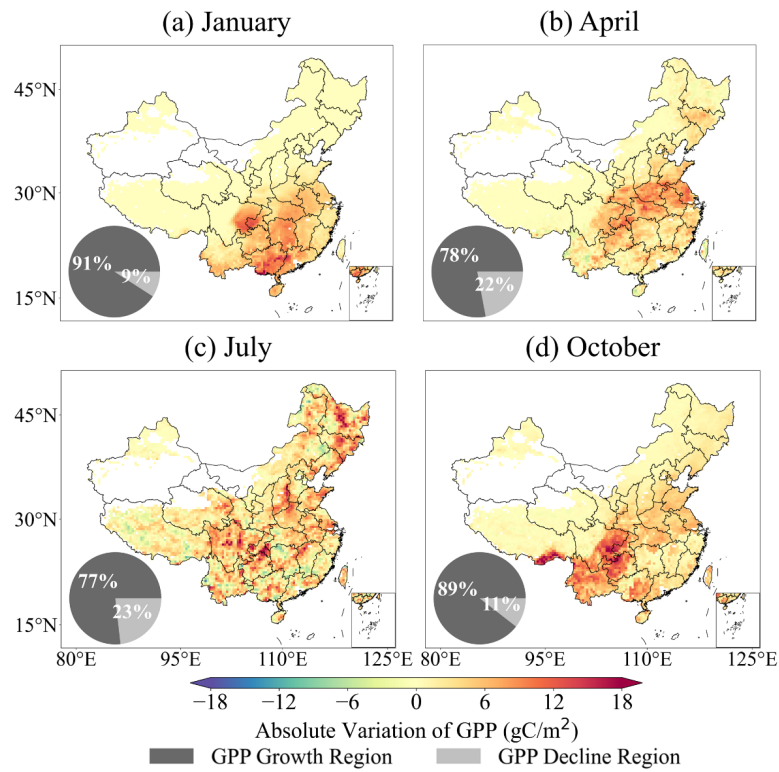


Figure 3. Impact of PER on GPP in gC/m^2 . Pie charts indicate the percentage of GPP change areas.

3.3. Dominant Meteorological Factors Driving the Projected Terrestrial GPP Variations

The main meteorological factors governing the variations in GPP influenced by global climate change were determined through sensitivity analyses, as depicted in Figure 4. In January, T_{min} and Srad dominate 66% (43%) and 34% (57%) of the study area under the SSP126 (SSP585) scenario, respectively. The regions dominated by Srad are predominantly located in southerly areas, such as the Yunnan, Guangxi, and Guangdong provinces. Notably, a transition from T_{min}-dominated to Srad-dominated influence occurs primarily within the SCB, Hubei, and Hunan provinces with the exacerbation of climate change. In April, approximately two-thirds of the study area exhibited variations in GPP driven by Srad, while one-fifth was influenced by T_{min} across all SSP scenarios. Regions characterized by T_{min} dominance were mainly situated in westerly areas with higher altitudes. It is worth mentioning that GPP variations in Yunnan Province are primarily influenced by VPD [47]. This finding can be attributed to increased VPD reducing stomatal conductance and impeding vegetation growth under the influence of climate change [46]. Moving on to July, around 80% of the study area was governed by Srad dominance, while VPD exerted control over approximately 20%. Notably, the NCP emerged as a prominent region dominated by VPD effects aligning with previous studies, highlighting significant correlations between ecosystem productivity and air moisture levels within this region [48,49]. Overall spatial patterns observed during April persisted in October; however, proportions of regions exhibiting Srad or VPD dominance decreased or increased correspondingly.

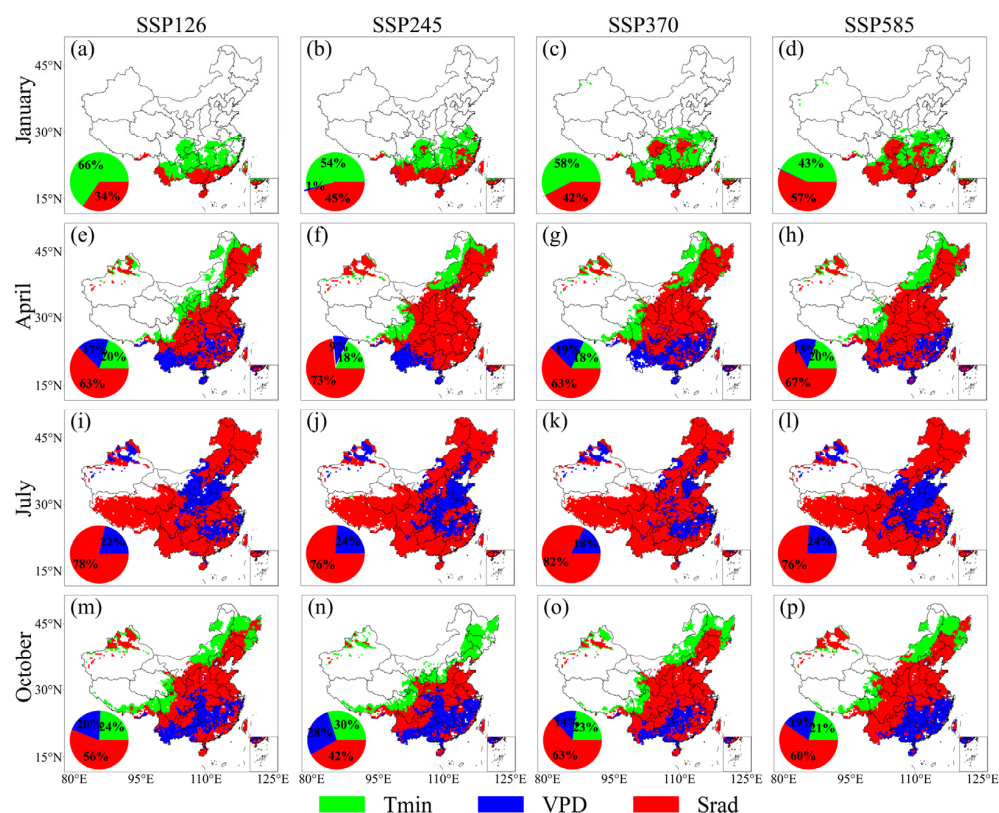


Figure 4. (a–p) Main factors cause GPP variations influenced by global climate change scenario. Pie charts indicate the proportions of the region occupied by the dominant factors.

The PER induces variations in pollutant concentrations, such as PM_{2.5} and O₃, which subsequently alter the meteorological parameters influencing GPP, including Srad, T_{min}, and VPD [50]. As presented in Table 3, due to a significant decrease in anthropogenic emissions, PM_{2.5} concentrations exhibit substantial reductions across all seasons, particularly in January (−49.22 μg/m³) and October (−18.31 μg/m³). These changes are mainly concentrated in heavily polluted regions [19], such as the NCP and SCB (see Figure S3). Declines

are also observed in O₃ concentrations but to a lesser extent ranging between −9.36 ppbv and −2.04 ppbv. The radiative effects of aerosol particles influence shortwave radiation reaching the surface [51,52] and modulate air temperature and VPD [53,54]. Increases of Sr_{ad} ranging from 0.27 MJ/m² to 1.18 MJ/m² are observed among different seasons. T_{min} exhibits more pronounced increases in January and October (0.15 °C and 0.19 °C) compared to April and July (only 0.06 °C and 0.03 °C). Correspondingly, more noticeable increases of VPD occur both in January and October either (22.77 Pa and 28.19 Pa), with an additional increase observed in July (16.80 Pa).

Table 3. Changes in meteorological factors and pollutant concentrations due to PER in China. An asterisk represents significant differences at a 95% confidence interval.

Variable	January	April	July	October
T _{min} (°C)	0.15 ± 0.22	0.06 ± 0.25	0.03 ± 0.23	0.19 ± 0.29
Sr _{ad} (MJ/m ²)	1.18 * ± 0.49	0.27 * ± 0.34	0.45 * ± 0.52	0.61 * ± 0.40
VPD (Pa)	22.77 * ± 14.77	0.02 ± 13.50	16.80 ± 30.10	28.19 * ± 24.03
PM _{2.5} (µg/m ³)	−49.92 * ± 25.52	−9.61 * ± 8.71	−7.55 * ± 8.82	−18.31 * ± 13.19
O ₃ (ppbv)	−2.04 * ± 6.35	−3.02 * ± 5.10	−9.36 * ± 5.72	−3.10 * ± 6.48

Sensitivity analyses reveal that Sr_{ad} is the primary driver governing variations in GPP throughout the year, with the exception of January when T_{min} takes precedence. In Figure 5, it can be observed that areas dominated by T_{min} account for 54% of the study area, primarily concentrated in Yunnan Province and central China in January. Conversely, Sr_{ad} dominates approximately 45% of the study area, mainly encompassing the Yunnan border, SCB, and southern China. The dominance of Sr_{ad} expands to cover 65%, 79%, and 54% of the study area in April, July, and October, respectively. On the other hand, proportions of areas dominated by T_{min} are found to be around 19% and 25% in April and October, respectively, but negligible in July. VPD-dominated regions occupy approximately 16% of the study area during April and 21% during both July and October, but are virtually absent in January and July. Spatially, T_{min}-dominated areas concentrate over central China and Yunnan Province in January, and extend to northeastern China, eastern Inner Mongolia, and the western Sichuan province in April and October. VPD-dominated regions focus primarily on southern China in April and October, and on central China in July.

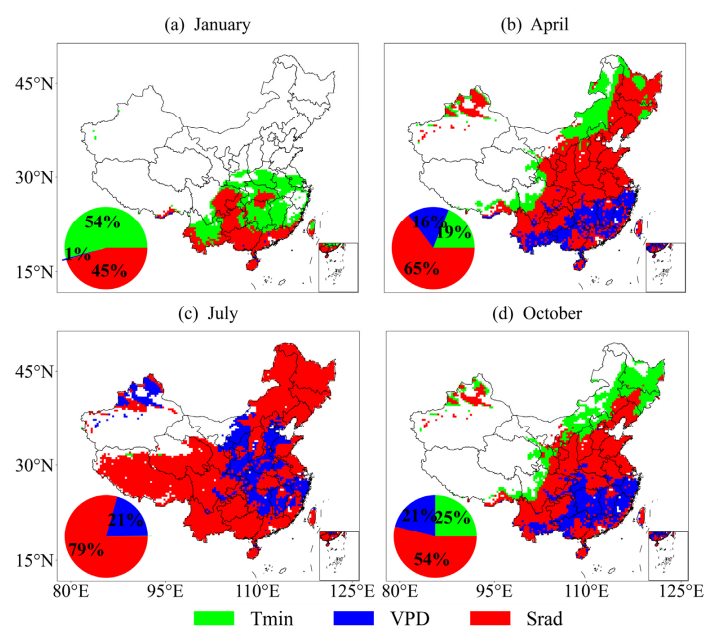


Figure 5. Main factors causing GPP variations influenced by carbon-neutral PER. Pie charts indicate the percentage of the region occupied by the dominant factors.

4. Discussion

Our findings indicate that global climate change impacts GPP negatively, which aligns with the results from the study by Mu et al. [55], and the implementation of carbon-neutral PER policies enhances vegetation carbon uptake in China (see Figure 1). Some studies have provided evidence for the positive impact of PER on GPP by examining the effects of aerosol and O₃ reduction on vegetation growth. For instance, Xu et al. found that reducing aerosol concentrations by 2030 benefits ecosystems [56]. Wang et al. indicated that lowering O₃ levels under the carbon neutrality goal will mitigate crop yield reductions caused by global climate change [57]. Furthermore, it is observed that aerosol radiative effects play a crucial role in promoting increased GPP under carbon-neutral PER policies. These effects are predominantly influenced by temperature variations during winter and shortwave radiation changes throughout other seasons. Specifically, the changes in T_{min} and Srad during January mitigate the adverse effects of low temperatures on vegetation [58], while the increase in Srad enhances the availability of PAR for plants. From a nationwide perspective, most regions within China have experienced an increase in GPP due to carbon-neutral PER policies (see Figure 3). Spatially, this enhancement is primarily concentrated in southwestern China and eastern China regions, where GPP is significantly affected by aerosols [59].

Several defects increase the uncertainties of GPP in this study. Firstly, the omission of considering the increase in atmospheric CO₂ concentration, despite its significant effects on the terrestrial carbon cycle [60–62], may lead to an underestimation of the decline in GPP caused by global climate change in 2060. The fertilization effect of elevated CO₂ levels on photosynthesis and vegetation growth is well recognized; however, it is important to note that this effect diminishes over time and may even shift towards a negative impact on GPP in the near future [12,13]. Therefore, the absence of the effect of CO₂ rise may underestimate the decline of GPP caused by global climate change in 2060, emphasizing the imperative role of offsetting from PER. Secondly, due to uncertainties associated with projected meteorological parameters, the reliability of estimated future GPP is limited. This study relies exclusively on data from the MPI-ESM1-2-HR model as a climate background field due to its favorable overall performance across evaluations of CMIP6 models [63]. However, there are evident discrepancies among different CMIP6 model data which can significantly affect simulation outputs for GPP. To assess this issue, meteorological data from 2016 of the other three CMIP6 models (see Table S5) are used for calculating China's GPP and compared against benchmark data (the MYD17A2H dataset). As shown in Table S6, results driven by the MPI-ESM1-2-HR model outperform those obtained using the other three CMIP6 models. Finally, current models used for estimating GPP exhibit substantial uncertainties [64,65]. The simplified models like MODIS-PSN can capture variations caused by meteorological parameters accurately enough; they failed to consider future changes in surface physical conditions or geochemical and physiological factors. Notably, PER-induced declines in O₃ concentrations might promote future increases in GPP [57], which have not been accounted for yet.

5. Conclusions

In this study, we conducted an estimation of the impacts of global climate change and pollutant emission reduction on GPP across China in 2060, with a focus on achieving carbon neutrality objectives. The findings reveal that carbon-neutral PER policies promote GPP growth in most regions of China in 2060, particularly during April and October, resulting in a total increase of at least 21.84 TgC compared to that in 2016, which offset the adverse effects of global climate change up to fourfold. Considering the coupled effects of carbon-neutral PER policies and global climate change, our analysis indicates that alterations in GPP patterns are primarily driven by global climate change but can be modulated through PER interventions. This suggests that the positive effects of carbon-neutral PER on China's terrestrial GPP can help alleviate the adverse impacts of climate change and mitigate the weakened CO₂ fertilization effect. This underscores the significance of adopting the

synergistic approach to air pollution control and carbon neutrality, thereby enhancing confidence in coordinated endeavors aimed at reducing pollutants and carbon emissions.

Supplementary Materials: The following supporting information can be downloaded at: <https://www.mdpi.com/article/10.3390/atmos15050578/s1>, Figure S1: Impact of global climate change on the spatio-temporal distribution of VPD in October; Figure S2: Coupled effects of carbon-neutral pollutant emission reduction policies and global climate change on GPP; Figure S3: Impacts of carbon-neutral pollutant emission reduction policies on PM_{2.5} and O₃ concentrations in China; Table S1: Error statistics of meteorological simulation results and observations; Table S2: Error statistics for the simulation results of PM_{2.5} and O₃ concentrations; Table S3: Impact of PER, global climate change and the coupled effect of these two factors on GPP in China; Table S4: Coupled effects of carbon-neutral pollutant emission reduction policies and global climate change on provincial GPP in China; Table S5: Information of the other three CMIP6 models; Table S6: Comparison of simulated GPP and benchmark values of each model in 2016.

Author Contributions: Conceptualization, G.S.; methodology, X.Q. and G.S.; software, X.Q.; investigation, X.Q., G.S. and F.Y.; writing—original draft preparation, X.Q.; writing—review and editing, G.S.; supervision, F.Y. All authors have read and agreed to the published version of the manuscript.

Funding: This research was funded by the National Key R&D Program of China, grant number 2023YFC3709301.

Institutional Review Board Statement: Not applicable.

Informed Consent Statement: Not applicable.

Data Availability Statement: The PM_{2.5} and O₃ concentrations are publicly available on the website of China National Environmental Monitoring Center via <https://air.cnemc.cn:18007/>, accessed on 2 November 2016. The meteorological parameters are publicly available on the website of China Meteorological Data Service Centre via <http://data.cma.cn/>, accessed on 2 November 2016. These data in the latest 7 days can be retrieved from these two websites. The authors routinely retrieved and processed relevant data. The MYD17A2H products are available through <https://ladsweb.modaps.eosdis.nasa.gov/missions-and-measurements/products/MYD17A2H>, accessed on 12 January 2024. The MPI-ESM1-2-HR data of the CMIP6 are available through <https://highresmpip.org/data/>, accessed on 15 March 2023.

Conflicts of Interest: The authors declare no conflicts of interest.

Abbreviations

BPLUT	Biome specified parameter look-up table
GPP	Gross primary productivity
LAI	Leaf area index
MFB	Mean fractional bias
MFE	Mean fractional error
NCP	North China Plain
NMB	Normalized mean bias
NME	Normalized mean error
NPP	Net primary productivity
PAR	Photosynthetically active radiation
PER	Pollutant emission reduction
PSN	Photosynthesis
RCPs	Representative concentration pathways
SCB	Sichuan Basin
Sra	Shortwave radiation
SSPs	Shared socioeconomic pathways
Tmin	Daily minimum temperature
VPD	Vapor pressure deficit
YGP	Yunnan–Guizhou Plateau
YSU	Yonsei University

References

- Niu, S.-L.; Chen, W.-N. Global change and ecosystems research progress and prospect. *Chin. J. Plant Ecol.* **2020**, *44*, 449. [[CrossRef](#)]
- Fang, J.-Y. Ecological perspectives of carbon neutrality. *Chin. J. Plant Ecol.* **2021**, *45*, 1173. [[CrossRef](#)]
- Lü, F.; Song, Y.; Yan, X. Evaluating carbon sink potential of forest ecosystems under different climate change scenarios in yunnan, southwest china. *Remote Sens.* **2023**, *15*, 1442. [[CrossRef](#)]
- Wang, Y.; Guo, C.-H.; Chen, X.-J.; Jia, L.-Q.; Guo, X.-N.; Chen, R.-S.; Zhang, M.-S.; Chen, Z.-Y.; Wang, H.-D. Carbon peak and carbon neutrality in china: Goals, implementation path and prospects. *China Geol.* **2021**, *4*, 720–746. [[CrossRef](#)]
- Beer, C.; Reichstein, M.; Tomelleri, E.; Ciais, P.; Jung, M.; Carvalhais, N.; Rödenbeck, C.; Arain, M.A.; Baldocchi, D.; Bonan, G.B. Terrestrial gross carbon dioxide uptake: Global distribution and covariation with climate. *Science* **2010**, *329*, 834–838. [[CrossRef](#)] [[PubMed](#)]
- Li, W.; Ciais, P.; Wang, Y.; Yin, Y.; Peng, S.; Zhu, Z.; Bastos, A.; Yue, C.; Ballantyne, A.P.; Broquet, G. Recent changes in global photosynthesis and terrestrial ecosystem respiration constrained from multiple observations. *Geophys. Res. Lett.* **2018**, *45*, 1058–1068. [[CrossRef](#)]
- Jingyun, F.; Jinhu, K.; Zhiyao, T.; Anping, C.E. Implications and estimations of four terrestrial productivity parameters. *Acta Phytocol. Sin.* **2001**, *25*, 414–419.
- Yuan, W.; Liu, S.; Yu, G.; Bonnefond, J.-M.; Chen, J.; Davis, K.; Desai, A.R.; Goldstein, A.H.; Gianelle, D.; Rossi, F. Global estimates of evapotranspiration and gross primary production based on modis and global meteorology data. *Remote Sens. Environ.* **2010**, *114*, 1416–1431. [[CrossRef](#)]
- Wang, Y.; Fu, B.; Lü, Y.; Chen, L. Effects of vegetation restoration on soil organic carbon sequestration at multiple scales in semi-arid loess plateau, china. *Catena* **2011**, *85*, 58–66. [[CrossRef](#)]
- Fernández-Martínez, M.; Vicca, S.; Janssens, I.A.; Ciais, P.; Obersteiner, M.; Bartrons, M.; Sardans, J.; Verger, A.; Canadell, J.G.; Chevallier, F. Atmospheric deposition, CO₂, and change in the land carbon sink. *Sci. Rep.* **2017**, *7*, 9632. [[CrossRef](#)]
- Zhu, Z.; Piao, S.; Myneni, R.B.; Huang, M.; Zeng, Z.; Canadell, J.G.; Ciais, P.; Sitch, S.; Friedlingstein, P.; Arneeth, A. Greening of the earth and its drivers. *Nat. Clim. Change* **2016**, *6*, 791–795. [[CrossRef](#)]
- Peñuelas, J.; Ciais, P.; Canadell, J.G.; Janssens, I.A.; Fernández-Martínez, M.; Carnicer, J.; Obersteiner, M.; Piao, S.; Vautard, R.; Sardans, J. Shifting from a fertilization-dominated to a warming-dominated period. *Nat. Ecol. Evol.* **2017**, *1*, 1438–1445. [[CrossRef](#)]
- Wang, S.; Zhang, Y.; Ju, W.; Chen, J.M.; Ciais, P.; Cescatti, A.; Sardans, J.; Janssens, I.A.; Wu, M.; Berry, J.A. Recent global decline of CO₂ fertilization effects on vegetation photosynthesis. *Science* **2020**, *370*, 1295–1300. [[CrossRef](#)]
- Cao, D.; Zhang, J.; Han, J.; Zhang, T.; Yang, S.; Wang, J.; Prodhon, F.A.; Yao, F. Projected increases in global terrestrial net primary productivity loss caused by drought under climate change. *Earth's Future* **2022**, *10*, e2022EF002681. [[CrossRef](#)]
- Yuan, W.; Zheng, Y.; Piao, S.; Ciais, P.; Lombardozi, D.; Wang, Y.; Ryu, Y.; Chen, G.; Dong, W.; Hu, Z. Increased atmospheric vapor pressure deficit reduces global vegetation growth. *Sci. Adv.* **2019**, *5*, eaax1396. [[CrossRef](#)] [[PubMed](#)]
- Zhang, S.; Worrell, E.; Crijns-Graus, W.; Wagner, F.; Cofala, J. Co-benefits of energy efficiency improvement and air pollution abatement in the chinese iron and steel industry. *Energy* **2014**, *78*, 333–345. [[CrossRef](#)]
- Yang, X.; Teng, F. The air quality co-benefit of coal control strategy in china. *Resour. Conserv. Recycl.* **2018**, *129*, 373–382. [[CrossRef](#)]
- Cheng, J.; Tong, D.; Zhang, Q.; Liu, Y.; Lei, Y.; Yan, G.; Yan, L.; Yu, S.; Cui, R.Y.; Clarke, L. Pathways of china's PM_{2.5} air quality 2015–2060 in the context of carbon neutrality. *Natl. Sci. Rev.* **2021**, *8*, nwab078. [[CrossRef](#)]
- Xu, B.Y.; Wang, T.J.; Li, S.; Zhuang, B.; Xie, M.; Li, M.; Xie, X. Assessment of the impact of “dual-carbon” goal on future changes in air pollution and climate in china. *Chin. Sci. Bull.* **2022**, *67*, 784–794. [[CrossRef](#)]
- Cheng, D.; Qi, G.; Song, J.; Zhang, Y.; Bai, H.; Gao, X. Quantitative assessment of the contributions of climate change and human activities to vegetation variation in the qinling mountains. *Front. Earth Sci.* **2021**, *9*, 782287. [[CrossRef](#)]
- Grell, G.A.; Peckham, S.E.; Schmitz, R.; McKeen, S.A.; Frost, G.; Skamarock, W.C.; Eder, B. Fully coupled “online” chemistry within the wrf model. *Atmos. Environ.* **2005**, *39*, 6957–6975. [[CrossRef](#)]
- Hong, S.-Y.; Noh, Y.; Dudhia, J. A new vertical diffusion package with an explicit treatment of entrainment processes. *Mon. Weather Rev.* **2006**, *134*, 2318–2341. [[CrossRef](#)]
- Chen, F.; Dudhia, J. Coupling an advanced land surface–hydrology model with the penn state–ncar mm5 modeling system. Part i: Model implementation and sensitivity. *Mon. Weather Rev.* **2001**, *129*, 569–585. [[CrossRef](#)]
- Grell, G.A. Prognostic evaluation of assumptions used by cumulus parameterizations. *Mon. Weather Rev.* **1993**, *121*, 764–787. [[CrossRef](#)]
- Morrison, H.; Thompson, G.; Tatarskii, V. Impact of cloud microphysics on the development of trailing stratiform precipitation in a simulated squall line: Comparison of one- and two-moment schemes. *Mon. Weather Rev.* **2009**, *137*, 991–1007. [[CrossRef](#)]
- Iacono, M.J.; Delamere, J.S.; Mlawer, E.J.; Shephard, M.W.; Clough, S.A.; Collins, W.D. Radiative forcing by long-lived greenhouse gases: Calculations with the aer radiative transfer models. *J. Geophys. Res. Atmos.* **2008**, *113*, D13103. [[CrossRef](#)]
- Gutjahr, O.; Putrasahan, D.; Lohmann, K.; Jungclaus, J.H.; von Storch, J.-S.; Brüggemann, N.; Haak, H.; Stössel, A. Max planck institute earth system model (mpi-esm1. 2) for the high-resolution model intercomparison project (highresmip). *Geosci. Model Dev.* **2019**, *12*, 3241–3281. [[CrossRef](#)]
- Zaveri, R.A.; Peters, L.K. A new lumped structure photochemical mechanism for large-scale applications. *J. Geophys. Res. Atmos.* **1999**, *104*, 30387–30415. [[CrossRef](#)]

29. Zaveri, R.A.; Easter, R.C.; Fast, J.D.; Peters, L.K. Model for simulating aerosol interactions and chemistry (mosaic). *J. Geophys. Res. Atmos.* **2008**, *113*, D13204. [[CrossRef](#)]
30. Horowitz, L.W.; Walters, S.; Mauzerall, D.L.; Emmons, L.K.; Rasch, P.J.; Granier, C.; Tie, X.; Lamarque, J.F.; Schultz, M.G.; Tyndall, G.S. A global simulation of tropospheric ozone and related tracers: Description and evaluation of mozart, version 2. *J. Geophys. Res. Atmos.* **2003**, *108*, D24. [[CrossRef](#)]
31. Emmons, L.K.; Walters, S.; Hess, P.G.; Lamarque, J.F.; Pfister, G.G.; Fillmore, D.; Granier, C.; Guenther, A.; Kinnison, D.; Laepple, T. Description and evaluation of the model for ozone and related chemical tracers, version 4 (mozart-4). *Geosci. Model Dev.* **2010**, *3*, 43–67. [[CrossRef](#)]
32. Li, M.; Liu, H.; Geng, G.; Hong, C.; Liu, F.; Song, Y.; Tong, D.; Zheng, B.; Cui, H.; Man, H. Anthropogenic emission inventories in china: A review. *Natl. Sci. Rev.* **2017**, *4*, 834–866. [[CrossRef](#)]
33. Zheng, B.; Tong, D.; Li, M.; Liu, F.; Hong, C.; Geng, G.; Li, H.; Li, X.; Peng, L.; Qi, J. Trends in china’s anthropogenic emissions since 2010 as the consequence of clean air actions. *Atmos. Chem. Phys.* **2018**, *18*, 14095–14111. [[CrossRef](#)]
34. Li, M.; Zhang, Q.; Kurokawa, J.-i.; Woo, J.-H.; He, K.; Lu, Z.; Ohara, T.; Song, Y.; Streets, D.G.; Carmichael, G.R. Mix: A mosaic asian anthropogenic emission inventory under the international collaboration framework of the mics-asia and htap. *Atmos. Chem. Phys.* **2017**, *17*, 935–963. [[CrossRef](#)]
35. Guenther, A.; Jiang, X.; Shah, T.; Huang, L.; Kemball-Cook, S.; Yarwood, G. *Model of Emissions of Gases and Aerosol from Nature Version 3 (megan3) for Estimating Biogenic Emissions*; Springer: Cham, Switzerland, 2020; pp. 187–192.
36. Boylan, J.W.; Russell, A.G. Pm and light extinction model performance metrics, goals, and criteria for three-dimensional air quality models. *Atmos. Environ.* **2006**, *40*, 4946–4959. [[CrossRef](#)]
37. Running, S.W.; Nemani, R.R.; Heinsch, F.A.; Zhao, M.; Reeves, M.; Hashimoto, H. A continuous satellite-derived measure of global terrestrial primary production. *Bioscience* **2004**, *54*, 547–560. [[CrossRef](#)]
38. Xiao, J.; Chevallier, F.; Gomez, C.; Guanter, L.; Hicke, J.A.; Huete, A.R.; Ichii, K.; Ni, W.; Pang, Y.; Rahman, A.F. Remote sensing of the terrestrial carbon cycle: A review of advances over 50 years. *Remote Sens. Environ.* **2019**, *233*, 111383. [[CrossRef](#)]
39. Running, S.W.; Zhao, M. Daily GPP and Annual NPP (mod17a2/a3) Products NASA Earth Observing System Modis Land Algorithm. MOD17 User’s Guide. Available online: https://www.nts.gov/umt.edu/files/modis/MOD17UsersGuide2015_v3.pdf (accessed on 3 May 2024).
40. Running, S.W. Global terrestrial gross and net primary productivity from the earth observing system. In *Methods in Ecosystem Science*; Springer: New York, NY, USA, 2000; pp. 44–57.
41. Hansen, M.C.; Reed, B. A comparison of the igbp discover and university of maryland 1 km global land cover products. *Int. J. Remote Sens.* **2000**, *21*, 1365–1373. [[CrossRef](#)]
42. Li, X.; Xiao, J. A global, 0.05-degree product of solar-induced chlorophyll fluorescence derived from oco-2, modis, and reanalysis data. *Remote Sens.* **2019**, *11*, 517. [[CrossRef](#)]
43. O’Neill, B.C.; Krieger, E.; Riahi, K.; Ebi, K.L.; Hallegatte, S.; Carter, T.R.; Mathur, R.; Van Vuuren, D.P. A new scenario framework for climate change research: The concept of shared socioeconomic pathways. *Clim. Change* **2014**, *122*, 387–400. [[CrossRef](#)]
44. Nossent, J.; Elsen, P.; Bauwens, W. Sobol’ sensitivity analysis of a complex environmental model. *Environ. Model. Softw.* **2011**, *26*, 1515–1525. [[CrossRef](#)]
45. Lu, Q.; Liu, H.; Wei, L.; Zhong, Y.; Zhou, Z. Global prediction of gross primary productivity under future climate change. *Sci. Total Environ.* **2024**, *912*, 169239. [[CrossRef](#)] [[PubMed](#)]
46. Novick, K.A.; Ficklin, D.L.; Stoy, P.C.; Williams, C.A.; Bohrer, G.; Oishi, A.C.; Papuga, S.A.; Blanken, P.D.; Noormets, A.; Sulman, B.N. The increasing importance of atmospheric demand for ecosystem water and carbon fluxes. *Nat. Clim. Change* **2016**, *6*, 1023–1027. [[CrossRef](#)]
47. Li, Y.; Shi, H.; Zhou, L.; Eamus, D.; Huete, A.; Li, L.; Cleverly, J.; Hu, Z.; Harahap, M.; Yu, Q. Disentangling climate and lai effects on seasonal variability in water use efficiency across terrestrial ecosystems in china. *J. Geophys. Res. Biogeosci.* **2018**, *123*, 2429–2443. [[CrossRef](#)]
48. Wu, X.; Zhang, R.; Bento, V.A.; Leng, S.; Qi, J.; Zeng, J.; Wang, Q. The effect of drought on vegetation gross primary productivity under different vegetation types across china from 2001 to 2020. *Remote Sens.* **2022**, *14*, 4658. [[CrossRef](#)]
49. Liu, M.; Yang, G.; Yuan, W.; Li, Z.; Gao, M.; Yang, Y.; Long, H.; Meng, Y.; Li, C.; Hu, H. Overridingly increasing vegetation sensitivity to vapor pressure deficit over the recent two decades in china. *Ecol. Indic.* **2024**, *161*, 111977. [[CrossRef](#)]
50. Law, B.E.; Falge, E.; Gu, L.; Baldocchi, D.D.; Bakwin, P.; Berbigier, P.; Davis, K.; Dolman, A.J.; Falk, M.; Fuentes, J.D. Environmental controls over carbon dioxide and water vapor exchange of terrestrial vegetation. *Agric. For. Meteorol.* **2002**, *113*, 97–120. [[CrossRef](#)]
51. Hu, B.; Zhao, X.; Liu, H.; Liu, Z.; Song, T.; Wang, Y.; Tang, L.; Xia, X.; Tang, G.; Ji, D. Quantification of the impact of aerosol on broadband solar radiation in north china. *Sci. Rep.* **2017**, *7*, 44851. [[CrossRef](#)] [[PubMed](#)]
52. Gao, M.; Han, Z.; Liu, Z.; Li, M.; Xin, J.; Tao, Z.; Li, J.; Kang, J.-E.; Huang, K.; Dong, X. Air quality and climate change, topic 3 of the model inter-comparison study for asia phase iii (mics-asia iii)—part 1: Overview and model evaluation. *Atmos. Chem. Phys.* **2018**, *18*, 4859–4884. [[CrossRef](#)]
53. Petäjä, T.; Järvi, L.; Kerminen, V.M.; Ding, A.J.; Sun, J.N.; Nie, W.; Kujansuu, J.; Virkkula, A.; Yang, X.; Fu, C.B. Enhanced air pollution via aerosol-boundary layer feedback in china. *Sci. Rep.* **2016**, *6*, 18998. [[CrossRef](#)]
54. Ou, S.; Wei, W.; Cai, B.; Chen, S.; Guan, P.; Cheng, S. The independent impacts of pm_{2.5} dropping on the physical and chemical properties of atmosphere over north china plain in summer during 2015–2019. *Sustainability* **2022**, *14*, 3930. [[CrossRef](#)]

55. Mu, Q.; Zhao, M.; Running, S.W.; Liu, M.; Tian, H. Contribution of increasing CO₂ and climate change to the carbon cycle in china's ecosystems. *J. Geophys. Res. Biogeosci.* **2008**, *113*, G01018. [[CrossRef](#)]
56. Yue, X.; Unger, N.; Harper, K.; Xia, X.; Liao, H.; Zhu, T.; Xiao, J.; Feng, Z.; Li, J. Ozone and haze pollution weakens net primary productivity in china. *Atmos. Chem. Phys.* **2017**, *17*, 6073–6089. [[CrossRef](#)]
57. Xu, B.; Wang, T.; Gao, L.; Ma, D.; Song, R.; Zhao, J.; Yang, X.; Li, S.; Zhuang, B.; Li, M. Impacts of meteorological factors and ozone variation on crop yields in china concerning carbon neutrality objectives in 2060. *Environ. Pollut.* **2023**, *317*, 120715. [[CrossRef](#)] [[PubMed](#)]
58. Bilska, A.; Sowiński, P. Closure of plasmodesmata in maize (*Zea mays*) at low temperature: A new mechanism for inhibition of photosynthesis. *Ann. Bot.* **2010**, *106*, 675–686. [[CrossRef](#)] [[PubMed](#)]
59. Xie, X.; Wang, T.; Yue, X.; Li, S.; Zhuang, B.; Wang, M. Effects of atmospheric aerosols on terrestrial carbon fluxes and CO₂ concentrations in China. *Atmos. Res.* **2020**, *237*, 104859. [[CrossRef](#)]
60. Levy, P.E.; Cannell, M.G.R.; Friend, A.D. Modelling the impact of future changes in climate, CO₂ concentration and land use on natural ecosystems and the terrestrial carbon sink. *Glob. Environ. Change* **2004**, *14*, 21–30. [[CrossRef](#)]
61. Walker, A.P.; De Kauwe, M.G.; Bastos, A.; Belmecheri, S.; Georgiou, K.; Keeling, R.F.; McMahon, S.M.; Medlyn, B.E.; Moore, D.J.P.; Norby, R.J. Integrating the evidence for a terrestrial carbon sink caused by increasing atmospheric CO₂. *New Phytol.* **2021**, *229*, 2413–2445. [[CrossRef](#)] [[PubMed](#)]
62. Schimel, D.; Stephens, B.B.; Fisher, J.B. Effect of increasing CO₂ on the terrestrial carbon cycle. *Proc. Natl. Acad. Sci. USA* **2015**, *112*, 436–441. [[CrossRef](#)]
63. Zhang, M.-Z.; Xu, Z.; Han, Y.; Guo, W. Evaluation of cmip6 models toward dynamical downscaling over 14 cordex domains. *Clim. Dyn.* **2022**, 1–15. [[CrossRef](#)]
64. Zhao, J.; Liu, D.; Zhu, Y.; Peng, H.; Xie, H. A review of forest carbon cycle models on spatiotemporal scales. *J. Clean. Prod.* **2022**, *339*, 130692. [[CrossRef](#)]
65. Zhao, Q.; Yu, L.; Li, X.; Peng, D.; Zhang, Y.; Gong, P. Progress and trends in the application of Google Earth and Google Earth Engine. *Remote Sens.* **2021**, *13*, 3778. [[CrossRef](#)]

Disclaimer/Publisher's Note: The statements, opinions and data contained in all publications are solely those of the individual author(s) and contributor(s) and not of MDPI and/or the editor(s). MDPI and/or the editor(s) disclaim responsibility for any injury to people or property resulting from any ideas, methods, instructions or products referred to in the content.